Plasma Chem Plasma Process (2017) 37:433–450
DOI 10.1007/s11090-016-9771-9

ORIGINAL PAPER

In-Situ Non-intrusive Diagnostics of Toluene Removal by a Gliding Arc Discharge Using Planar Laser-Induced Fluorescence

Jinlong Gao[1] · Jiajian Zhu[1,2] · Andreas Ehn[1] · Marcus Aldén[1] · Zhongshan Li[1]

Received: 16 July 2016 / Accepted: 1 December 2016 / Published online: 10 December 2016

Abstract A non-equilibrium gliding arc discharge anchored on two diverging stainless steel electrodes was extended into open air by a toluene-containing air jet. The removal process of the toluene by the non-equilibrium gliding arc discharge was investigated through in situ and non-intrusive laser-based techniques. Simultaneous planar laser-induced fluorescence (PLIF) of toluene and OH radicals were employed to achieve on-line visualization of the toluene decomposing process by the gliding arc discharge column. Toluene PLIF images with high spatial and temporal resolution showed that the non-equilibrium plasma of the gliding arc discharge is effective in decomposing toluene molecules. Instantaneous toluene removal efficiency was estimated from the toluene PLIF images, showing that the initial toluene concentrations and oxygen concentrations affected the toluene removal efficiency. The toluene removal efficiency decreased with the initial toluene concentration, whereas the efficiency increased with the oxygen concentration. The OH generation in the discharge was found to be enhanced with an increase of the toluene concentration from the OH PLIF results. The relative instantaneous distribution between the OH produced from the discharge channels and the toluene flow was simultaneously visualized. The instantaneous distributions of toluene and OH radicals that were acquired simultaneously by PLIF, were well complementary, suggesting that radicals generated by the gliding arc discharge were responsible for toluene removal in the active volume of the gliding arc discharge. The effective width of the plasma volume for the toluene removal were measured, which gives a new insight into the optimization of industrial design for practical gliding arc reactors.

Keywords Flue-gas treatment · Toluene · Non-equilibrium plasma · PLIF · Volatile organic compounds (VOCs)

✉ Zhongshan Li
zhongshan.li@forbrf.lth.se

[1] Division of Combustion Physics, Lund University, P.O. Box 118, 221 00 Lund, Sweden

[2] Present Address: Science and Technology on Scramjet Laboratory, National University of Defense Technology, Changsha 410073, China

Introduction

Toluene ($C_6H_5CH_3$) is a typical volatile organic compounds (VOCs), emitted from the volatilization of petroleum oil, motor vehicle exhaust and organic solvents and thinners. Due to an adverse effect on the environment and public health, it is of vital importance that the emissions of this compound can be controlled [1, 2]. Non-thermal plasmas have shown a strong potential for the reduction of gaseous pollutant emissions such as NO_x [3, 4], H_2S [5, 6], PAH [7] and VOCs [8, 9]. A gliding arc discharge as one of the non-thermal plasma sources, can provide active environments with high electron temperature and low gas temperature. Most of its energy could effectively contribute to producing favorable species for pollutant removal instead of heating the gas [10, 11]. Energetic electrons, excited atoms, activated molecules and reactive radicals, such as O, N, OH and N_2*, generated from the plasma discharge column [12, 13], can react with the toluene molecules and decompose them into small molecules, like CO_2, CO and H_2O [14, 15]. Compared with conventional VOCs abatement technology, such as liquid absorption, activated carbon absorption and catalytic oxidation etc., good selectivity and high energy efficiency make gliding arc discharges more attractive for toluene decomposition [14, 16, 17].

A series of studies have been performed to investigate the performance of gliding arc discharges as tools for removing pollutants. Early in the 1990s, Czernichowski applied the gliding arc discharge to the environmental control industry [5]. Using a sampling analysis method with gas chromatography (GC) for the entry and exit of a gliding discharge reactor, it was found that the toluene concentration could be reduced from 1800 to 140 ppm with low energy consumption by the gliding arc discharge. Du et al. [14] also demonstrated that a gliding arc discharge reactor can decompose toluene effectively. In order to understand the removal process of toluene by the non-equilibrium discharge, the sampling analysis methods, such as FTIR and GC have been extensively applied to analyze the products and by-products of the toluene treatment by the non-equilibrium discharge. The influences on the toluene removal efficiency from water vapor, oxygen content and initial toluene concentration have been investigated separately using these sampling methods to reveal the mechanism of toluene decomposition by non-thermal plasmas. It has been demonstrated that the toluene removal efficiency is strongly influenced by the humidity and oxygen content [14, 16]. The high initial water vapor concentration in the gas stream was found to be in favor of promoting toluene decomposition [16]. It is believed that the radical reactions are crucial in the toluene decomposition process. Oxygen derived radicals from the electron dissociation of gliding arc discharge, like O, OH and ozone etc., played a dominant role in the process of toluene decomposition [18]. Effects of the initial toluene concentration on the toluene removal efficiency and energy efficiency have also been studied with the GC analysis method [17]. Kinetic models were also built to have a better understanding of the mechanism of toluene decomposition by non-thermal discharges [19, 20]. In pure nitrogen, the main channels of toluene decomposition are associated with the metastable N_2 ($A^3\sum_u^+$) and N_2 ($a^1\sum_u^-$) nitrogen molecules, as suggested by the kinetic model of Trushkin [19]. However, the hydroxyl radical (OH) was recognized as the dominant radical to react with toluene molecules in the conditions when water was presented [20].

The above-mentioned studies have provided an in-depth investigation on toluene removal with non-thermal plasma [7–19]. However, most experimental work focused on the use of sampling methods to measure the concentration of the gas components. As the sampling method is limited to the analysis of the gas stream before and after the discharge

reactor, the toluene decomposition process in the discharge volume is mainly deduced from the off-line product and by-product composition comparison before and after the discharge system. In addition, the gliding discharge for pollutant removal is usually operated in turbulent flows, which would influence the dynamics of the discharge significantly. How the gliding discharge channel interacting with the toluene flow is still unrevealed. Therefore, an in situ and non-intrusive visualization of the instantaneous reaction process of toluene and plasma volume could enhance the understanding of the toluene removal process by the non-equilibrium plasma, which is the aim of this paper.

Planar laser-induced fluorescence (PLIF) imaging utilizes a short-pulsed laser ($\sim$5 ns) and a fast-gated camera ($\sim$30 ns) enabling instantaneous imaging for the flow reaction system. This instantaneous image can visualize the distribution of reactive radicals and pollutant molecules in the turbulent flow and the discharge reaction system can be considered as frozen in time. As OH is a representative active radical generated by the plasma discharge channel, it can be used as a marker for the plasma channel. PLIF of toluene and OH have been extensively developed and applied in the combustion field [21–24], hence, it is feasible to be applied to the visualization of toluene in plasma reaction system.

In the present study, in situ and non-intrusive measurements on the toluene removal process by the non-equilibrium plasma were conducted in a gliding arc discharge system based on PLIF of toluene and OH. Firstly, single-shot PLIF images of toluene with high spatial and temporal resolution were obtained, which enabled the toluene flow across the plasma column to be visualized. Secondly, PLIF of toluene and OH were implemented simultaneously to reveal the relative distribution between the arc channel and toluene molecules in a turbulent flow. On-line measurements of the reaction process including the plasma channel and toluene stream were achieved. Based on the in situ information obtained with PLIF, the toluene removal efficiency and the effective width of the plasma volume were non-intrusively measured.

Experimental Method

Gliding Discharge System

As shown in Fig. 1, the experimental setup consisted of two parts: the gliding arc system and the PLIF measurement system. The gliding arc discharge system used here was similar to the one used in our previous works [10, 25, 26] and only a brief description is given here. Two internally water-cooled, diverging stainless steel electrodes were fixed on a Teflon plate, as shown by the inserted direct image in Fig. 1. To ensure a free propagation of the gliding arc channel and avoid surface discharge, this setup was placed in open atmosphere condition. An alternating current (AC) power generator (Generator 9030E, SOFTAL Electronic GmbH, Germany) was used to supply 35 kHz high voltage to the two electrodes. The plasma column was formed from the discharge between the two electrodes. The rated output power of the generator was kept at 800 W throughout the study.

The gliding discharge column was extended downstream by an air jet from a 3 mm diameter hole in between the two electrodes on the Teflon plate. The air supplied to the discharge system was delivered from two channels, of which the flow rates were independently regulated by mass flow controllers (Bronkhorst). The air flow in one channel, after the mass flow controller, passed through a toluene-contained bubbler (temperature controlled at 25 $\pm$ 1 °C) to carry out saturated toluene vapor at the set temperature.

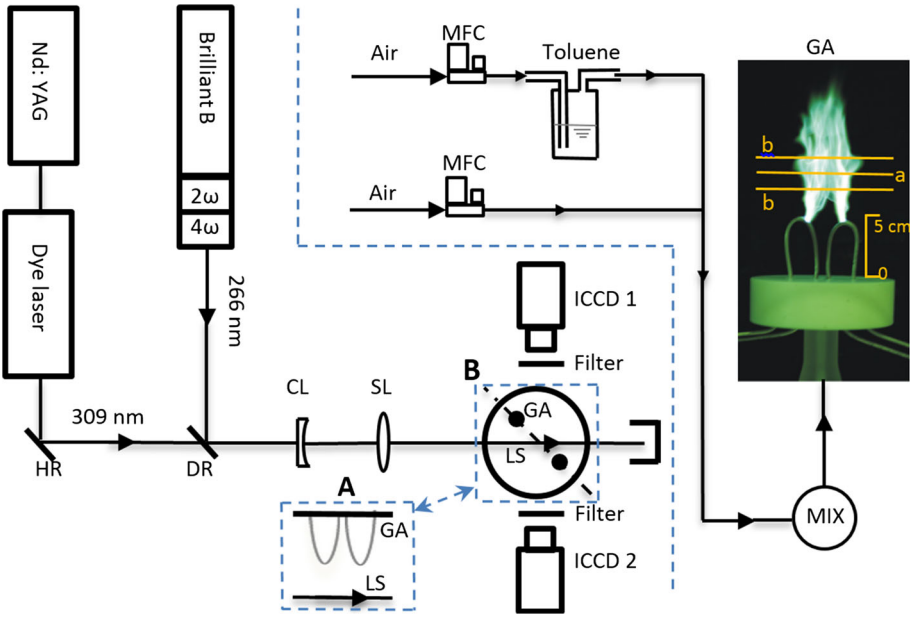

Fig. 1 Experimental setup for simultaneous PLIF of toluene and OH in the toluene removal by a gliding arc discharge. *HR* high reflective mirror, *DR* Dichroic mirror, *CL* cylindrical lens (−40 mm), *SL* spherical lens (300 mm), *MFC* mass flow controller, *GA* gliding arc, *LS* laser sheet. A typical gliding discharge image recorded by a Canon camera with 1/30 s exposure time is shown to the right. Sketches in *dash squares* A and B show the *top views* for two configurations of the alignment between laser sheet and discharge system

Subsequently, the toluene/air mixture mixed with the pure air from the other channel before the entrance into the discharge system. The total flow rate in the whole study was kept at 14 standard liters per minute (SLM) and remained unchanged. By varying the flow rate fraction of the air/toluene channel from 0 to 1, the relative initial toluene concentration was regulated from 0 to 3.74%. The concentration values were estimated from the saturated toluene vapor pressure at 25 °C and 1 atm.

Our previous study has shown that the characteristics of the discharge is strongly related with the flowrate [10]. Higher flow rate leads to larger turbulent convection cooling and stronger turbulent eddies. It has also been shown that a sustained diffusive gliding discharge in large volume can be obtained under optimized coupling of the flow rate and power [26].

The voltage and current waveform of the discharge system was monitored by a voltage probe (Tektronix P6015A) and a current monitor (model 6585, Pearson Electronics), respectively. A typical waveform of the measured current and voltage of the gliding discharge are shown in Fig. 2. As shown in Fig. 2a, the current through the gliding arc discharge channel was around several hundreds of milliamperes (mA) and there was no spark appearing during operation. This indicated that a sustained diffusive gliding arc discharge was obtained with the flow rate (14 SLM) and power (800 W) that was used in this study [26]. This kind of diffusive gliding arc discharge was mainly operated in the glow mode which shows non-equilibrium characteristics, in which the electron temperature was much higher than the gas temperature and large amount of active radicals were generated.

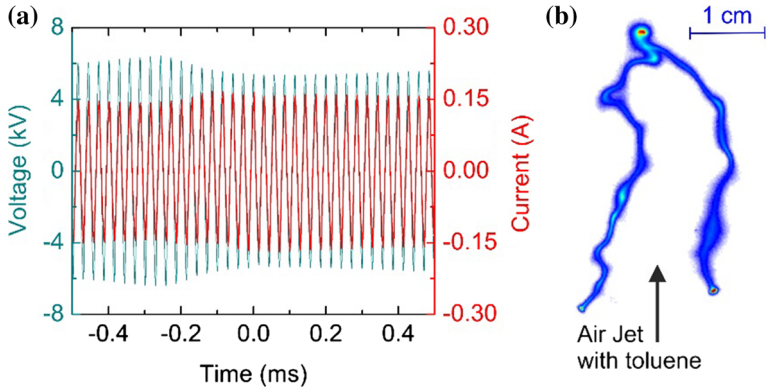

Fig. 2 **a** A typical voltage and current waveform of the gliding arc discharge; **b** A photo of the discharge channel (14.04 us exposure time)

An instantaneous photo (14.04 μs exposure time) of the gliding discharge, recorded by a high-speed video camera (FASTCAM SA5, Photron) is shown in Fig. 2b. The emissions of the discharge channel were mainly from N_2* [25]. It demonstrated that the non-equilibrium discharge has a string-like channel. This channel, with an approximate radius of 1 mm, is anchored on two electrodes propagate downstream of the air jet. It can be seen that the discharge channel is wrinkled and distorted by the local turbulent flow. To visualize the local distribution of the wrinkled discharge channel and the local turbulent toluene flow, simultaneous OH and toluene planar laser-induced fluorescence imaging were performed in this study.

The Planar Laser-Induced Fluorescence (PLIF) System

A schematic diagram of the optical setup for performing PLIF investigation is illustrated in Fig. 1 together with the gliding discharge system. For toluene PLIF measurements, the 266 nm laser beam from the 4th harmonic of an Nd:YAG laser (Brilliant B, Quantel) was used to approach the S_0–S_1 (π, π*) transition for the excitation of toluene molecules. The laser beam has a pulse width of 5 ns and pulse energy of 65 mJ. An intensified CCD camera (PIMAX II, Princeton Instrument) with a resolution of 1024 × 1024 pixels was used to collect the toluene fluorescence signal. The Q-switch signal from the laser was used to trigger the camera gate (30 ns). A Liquid *N*-dimetylformamid filter with 12 mm thickness was installed before the camera to suppress scattered laser light. A frequency-doubled, Nd:YAG-pumped dye laser (Sirah) with Rhodamine 610 and Rhodamine 640 dissolved in ethanol as dye, was tuned to 309 nm to excite the $Q_1(6)$ line of the OH ($A^2\sum^+ \rightarrow X^2\Pi, (0,0)$) band which has the least temperature dependence. To avoid the cross talk with toluene, the 309 nm band was selected instead of that at 284 nm. The pulse duration of the 309 nm laser was 5 ns and the pulse energy was around 25 mJ. The laser wavelength was scanned and compared with a simulated spectrum using LIFBASE to identify the proper OH lines for excitation. OH PLIF images were recorded by a PIMAX I camera with a resolution of 512 × 512 pixels. The camera gate (30 ns) was synchronized with the laser pulses from the Nd:YAG laser. An OH filter (Semrock OH, 320/40) was installed in front of the PIMAX I camera to suppress scattered laser light and plasma emission from the gliding arc.

A dichroic mirror for 266 nm was used to spatially overlap the 266 nm and 309 nm laser beams. The overlapped laser beams were expanded in vertical direction into a laser sheet ($\sim 50\,\text{mm} \times 0.5\,\text{mm}$) using one $f = -40$ mm cylindrical lens and one $f = +300$ mm spherical lens. The laser sheet was guided through the discharge region to visualize the interaction between the plasma column and the toluene flow. Two ICCD cameras were aligned perpendicular to the laser sheet and opposed to each other as shown in Fig. 1. A signal generator (DG575, Stanford Research Systems) was used to synchronize the two lasers. A time separation of 100 ns was set for the two laser pulses to minimize cross talk between the two image acquisitions, which was verified from experiments. As the time shift was short compared with the characteristic time scale of the flow (~ 100 μs, estimated time for the discharge channel moving for 1 mm), the system can still be regarded as static. Cross talk evaluation was performed by blocking one laser once and checking the corresponding camera. The evaluation showed that there was no detectable cross talk. Based on the recorded images using the two cameras for the same grid target, pixel to pixel corrections for the two cameras were achieved. The arrow in Fig. 2b shows the direction of the toluene flow and the overall direction of propagation for the arc channel.

In order to visualize the flow reaction system from different angles, the discharge setup was aligned in two kinds of configurations with the laser sheet kept standing in vertical direction. In configuration A, the Teflon plate together with the electrodes were aligned horizontally and the discharge channel propagated towards the camera with the flow. Top view of this configuration is shown in the dash square A in Fig. 1. In this configuration the laser sheet was cross perpendicular to the jet flow. Relative position of the laser sheet to the discharge systems was shown with a yellow line *a* shown in the direct image in Fig. 1. The distance between the laser sheet and the Teflon plate surface was 9 cm. As in the investigated conditions, the jet flow velocity is high (34 m/s), the buoyancy effect only exists on the downstream part of the channel. In configuration B the Teflon plate with the electrodes was placed vertically and the discharge channel propagated upwards with the flow. Top view of this configuration is shown in dash square B in Fig. 1. The laser sheet passed through the discharge channel and the side view of the laser sheet was the plane between the two yellow lines marked with *b*–*b* in Fig. 1. In this configuration, to improve the probability of hitting the discharge channel by the laser sheet, the laser sheet passed in between the two electrodes and had a 45° angle with the plane containing the two electrodes.

Results and Discussion

Toluene PLIF

Figure 3 shows single-shot toluene PLIF images (a, b) and averaged toluene PLIF images (c, d). These images were recorded when the discharge system were aligned as in configuration A, in which the laser sheet was perpendicular to the direction of the gas flow. The laser sheet was kept at 9 cm away from the Teflon plate. Background images recorded in the same flow condition with the laser off have been subtracted from the raw PLIF images. Laser-induced fluorescence is linearly proportional to the number density of the excited molecules and is influenced by laser intensity and quenching rate of the excited species [21]. Toluene PLIF image correction due to laser intensity profile has been

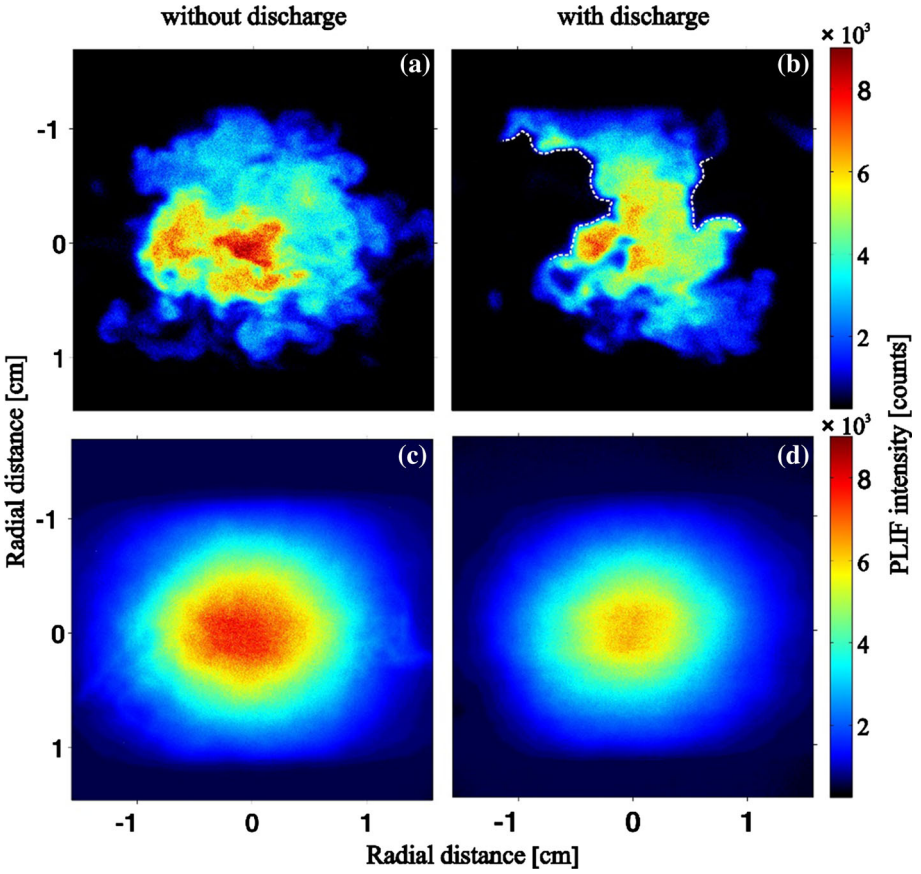

Fig. 3 Toluene PLIF images recorded for a 1.25% toluene-contained air flow when the discharge system were aligned as configuration A. The distance of the laser sheet to the Teflon plate is 9 cm. **a** Single-shot toluene PLIF image when the discharge was off; **b** Single-shot toluene PLIF image when the discharge was on; **c** 200-frames-averaged toluene PLIF image without discharge; **d** 200-frame averaged toluene PLIF image with discharge

implemented based on the Rayleigh profile of the laser sheet. Quenching effects of the toluene fluorescence is mainly related with oxygen concentration and temperature [21, 24]. Considering the relatively low concentration of toluene and low-ionization degree of the gliding discharge, the concentration of oxygen was treated as constant. As shown in our previous work, the high temperature region (>500 K) of the gliding arc discharge is distributed in the vicinity of the plasma column and restrained in a narrow region [27] where there are relatively more energetic electrons and reactive radicals distributed in this core region. It is expected that the toluene molecules are more effectively destructed in this core region. Therefore, the toluene LIF intensity can be used to qualitatively represent the toluene concentration, and the distribution of toluene concentration is represented by the toluene PLIF image. The influence of the temperature distribution would be examined again when we deal with single-shot toluene PLIF images.

Single-shot toluene PLIF image as shown in Fig. 3a was recorded for the air stream containing the toluene concentration of 1.25% when the gliding arc was absent. The

instantaneous spatial distribution of the toluene has been illustrated. The toluene PLIF signal had the highest intensity in the central part where the air jet originated and distributed evenly around the center. As the PLIF images show, toluene molecules had distributed into a 2×2 cm^2 region, where the toluene LIF intensity was 3 orders of magnitudes higher than the surroundings. The single-shot PLIF image recorded with the discharge on is shown in Fig. 3b. It is obvious to see that the toluene PLIF signal with high intensity (>500 counts) was distributed in a smaller region compared with Fig. 3a. There were sharp edges clearly appearing at the two sides of the toluene region which have been marked out with the white dash curves. The region half-wrapped with white dash curves indicates where the discharge channel penetrated through the laser sheet. Different reactive species initiating the decomposition of toluene molecules through the reactions R1–R10, such as energetic electrons, ions and free radicals, were generated from the discharge channel [28, 29]. These reactive species would be transported into the toluene region and react with toluene molecules as a result of turbulence. Hence, the toluene concentration decreased and led to a region with low intensity of toluene PLIF signal.

$$C_6H_5{\cdot}CH_3 + e^- \rightarrow C_6H_5 + CH_3 + e^- \quad \text{(R1)}$$

$$C_6H_5{\cdot}CH_3 + e^- \rightarrow C_6H_4 + CH_3 + H + e^- \quad \text{(R2)}$$

$$C_6H_5{\cdot}CH_3 + e^- \rightarrow C_5H_6 + C_2H_2 + e^- \quad \text{(R3)}$$

$$C_6H_5{\cdot}CH_3 + e^- \rightarrow C_3H_4 + C_4H_4 + e^- \quad \text{(R4)}$$

$$C_6H_5{\cdot}CH_3 + O^+, O_2^+, N^+, \text{or } N_2^+ \rightarrow C_6H_4 + CH_3^+ + O, O_3, N, \text{or } O_2 \quad \text{(R5)}$$

$$C_6H_5{\cdot}CH_3^+ + e^- \rightarrow C_6H_5 + CH_3 \quad \text{(R6)}$$

$$C_6H_5{\cdot}CH_3 + N_2\left(A^3\textstyle\sum_u^+\right) \rightarrow C_6H_5 + CH_3 + N_2 \quad \text{(R7)}$$

$$C_6H_5{\cdot}CH_3 + N_2\left(a^1\textstyle\sum_u^-\right) \rightarrow C_5H_6{\cdot}CH_3 + C_2H_2 + N_2 \quad \text{(R8)}$$

$$C_6H_5{\cdot}CH_3 + N_2\left(A^3\textstyle\sum_u^+\right) \rightarrow C_6H_5{\cdot}CH_2 + H + N_2 \quad \text{(R9)}$$

$$C_6H_5{\cdot}CH_3 + N_2\left(A^3\textstyle\sum_u^+\right) \rightarrow C_6H_4{\cdot}CH_3 + H + N_2 \quad \text{(R10)}$$

Estimation of Toluene Removal Efficiency

The toluene PLIF images shown in Fig. 3c and d are averaged over 200 frames. It is clearly seen that the toluene LIF intensity decreased in the presence of the gliding arc discharge. A toluene removal ratio can be estimated with the averaged value of Fig. 3d divided by Fig. 3c. As all the measurements were taken with the same flow rate and the discharge only had minor influence on the flow field, the estimation of toluene removal efficiency by this ratio method will not be affected by the toluene diffusion. Note that, this removal ratio is the planar efficiency of one single channel plasma. Considering the volumetric effect and multi-channel geometry generally adopted in industrial applications, this efficiency would be much higher. This toluene removal ratio can qualitatively characterize the removal capacity of the single gliding discharge channel.

Figure 4 shows the averaged ratio of the removed toluene with a discharge at different initial toluene concentrations. It can be seen that the toluene removal ratio is decreasing with the inlet toluene concentration. The product of the toluene removal ratio and the initial toluene concentration is also plotted in Fig. 4. As the flow rate in the study is constant, this product is linearly proportional to the absolute amount of the toluene molecules removed. On the contrary to the decrease of toluene removal ratio, the increased initial toluene concentration lead to larger amount of toluene molecules decomposed, as shown in Fig. 4. It also means that the energy efficiency for decomposing toluene molecules was increased as the total energy deposit was kept constant. This trend is also found in a rotating discharge reactor [17].

In addition to the averaged planar toluene removal efficiency, instantaneous local removal efficiency by the gliding discharge channel was also examined. Single-shot toluene PLIF images with high spatial resolution can be employed to estimate the instantaneous local toluene removal efficiency by the gliding discharge channels. A typical single-shot PLIF image and cross-sectional intensity distribution is presented in Fig. 5. The intensity of the toluene PLIF signal is represented by the color bar. This PLIF image was recorded in configuration B where the discharge channel propagated upward.

It is clearly shown from the PLIF image that toluene is distributed into two regions with significant contrast of PLIF intensity level. In the central region, the toluene PLIF signal has a low intensity level close to 0, while the signal is as high as thousands of counts further away from the discharge channel. Therefore, a threshold of 500 counts was chosen to divide the image into two regions: L region where the toluene PLIF intensity is lower than 500 counts and H region where the toluene PLIF intensity is above 500 counts. Figure 5 shows that the L region located in the central part of the image. For most parts inside this region the toluene PLIF intensity is close to 0. The L region indicates where the toluene was totally decomposed and the discharge channel presented. The H region distributed around the L region has an averaged intensity level of around 5000 counts indicating the region where toluene was not influenced by the discharge channel.

To estimate the local removal efficiency by the discharge channel, dashed lines which pass through the L region were drawn in Fig. 5. Vertical and horizontal cross-sectional intensity distributions were calculated by summing up the intensity inside the dashed lines area (10 pixels wide) along the vertical direction and horizontal direction, respectively. The vertical and horizontal cross-section profile have been shown at left side and down side,

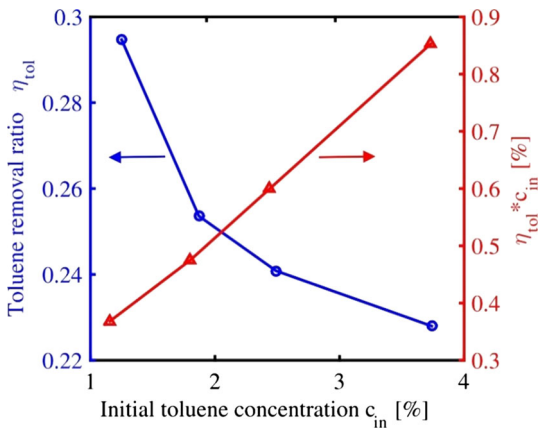

Fig. 4 Dependence of averaged toluene removal efficiency η_{tol} and the product of η_{tol} with toluene concentration c_{in} on initial toluene concentration c_{in}

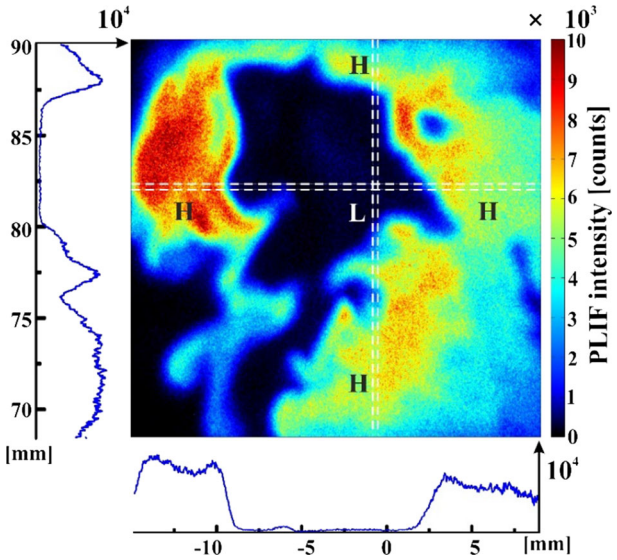

Fig. 5 Single-shot toluene PLIF image and cross-sectional intensity distribution for a 1.25% toluene-contained air flow recorded with the discharge system aligned as in configuration B. (*Left*) vertically cross-sectional intensity distribution, (*lower*) horizontally cross-sectional intensity distribution. *L* low intensity region (<500 counts); *H* high intensity region (>500 counts)

respectively, in Fig. 5. A scalar arrow which is equal to 10^4 counts has been put on each end of the two cross-sectional curves. It can be seen from the curves that the toluene PLIF intensities inside the L region close to 0 for both curves. The low intensity of toluene PLIF are caused by the effective decomposition of toluene molecules by the discharge channel. If we consider the homogeneity of the toluene distribution without the gliding discharge, the toluene concentration in the L region should be commensurate with the surroundings before the discharge channel present. As a result, it is plausible to use the average toluene LIF intensity of the region (H region in Fig. 5), where the discharge channel has little influence and the toluene LIF intensity is higher, to represent the toluene level before the presence of the discharge channel. The local toluene removal efficiency around the discharge column is estimated from the ratio between the average toluene PLIF intensity value of the L region and H region.

For the single-shot toluene PLIF image shown in Fig. 5, this ratio is calculated as 0.07 which represents the residual toluene ratio with the presence of discharge channel, and thus the local toluene removal efficiency due to the discharge channel is estimated to be up to 93%. This local toluene removal efficiency has been checked in other single-shot PLIF images recorded in the same condition as well. The mean value of the local toluene removal efficiency around the arc channel is measured to be around 95.1%, and the standard deviation of 3%.

Since the temperature has a reducing influence on the toluene fluorescence quantum yield, the toluene PLIF signal intensity will decrease with the increasing temperature [22]. The influence of temperature on the estimation of local toluene removal efficiency has been examined here. In our previous work, Rayleigh thermometry was conducted on a same type of gliding discharge [27]. It is found that the maximum temperature around the discharge channel reached about 1100 K. The high temperature region (>500 K) spread

across the discharge channel for about 3–5 mm. If the temperature influence on toluene LIF quenching is considered, the toluene fluorescence signal should be enhanced. Considering the high temperature distribution, the intensity correction was performed on a 7.5 mm wide region (−7.5–0 mm) in the horizontal profile of Fig. 5. A correction factor of 10 was used according to the measurement of toluene fluorescence quantum yield dependence on temperature in [22]. The local toluene removal efficiency estimated after the correction was 92.3%. The difference induced by the temperature influence, 0.7% is smaller than the standard deviation among different shots. The reason for that the temperature only had minor effect on the estimation of removal efficiency is that the toluene LIF intensity in most part of the L region is as low as 0. In all, as the temperature variation induced only negligible effect on the estimation of toluene removal efficiency, the temperature effect was neglected in the following discussion for simplification.

Even though the local removal efficiency around the arc channel is quite high, the overall removal efficiency of a toluene flow treatment discharge reactor is usually lower. The reason is that the region with high toluene removal efficiency is restrained in a limited region around the discharge channel. The width of this limited region is a crucial characteristic of the discharge which influences the overall toluene removal efficiency. For convenience, the effective width is defined here, which means the width of the region where the species generated from the discharge channel results in toluene decomposition with high efficiency (>70%). As estimated from the toluene PLIF image in Fig. 5, the effective width is about 11.5 mm. It is believed that the effective width is highly related with the diffusion of radicals produced from the discharge channel.

OH PLIF

OH as one of the representative active radicals generated in the gliding arc discharge is considered to play an important role in the toluene decomposition [20, 30]. OH PLIF study was implemented to reveal the distribution of reactive radicals in the toluene removal process. Single-shot OH PLIF images with 1.25% toluene contained in the flow and with no toluene contained are shown in Fig. 6, where the configuration A as shown in Fig. 1 was adopted to make the laser sheet cut through the plasma channel. The distance of the

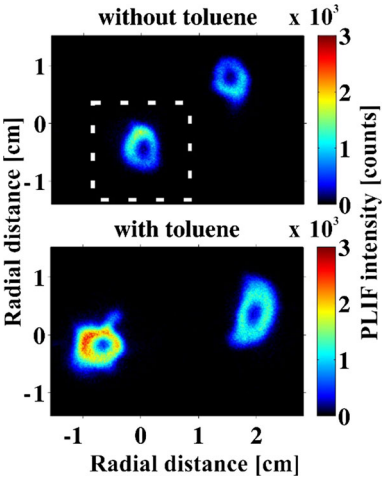

Fig. 6 Single-shot OH PLIF images recorded in the discharge for the flow without toluene contained and with 1.25% toluene contained, respectively. The laser sheet and the discharge system were aligned as in Configuration A

laser sheet to the Teflon plate was kept at 9 cm, same as for toluene PLIF. A hollow structure is obviously shown both in the cases with and without toluene which has also been observed in our previous work [10, 25]. OH PLIF images presented in Fig. 7 were recorded with the discharge system aligned as configuration B, where the laser sheet is parallel to the arc-moving direction. In a similar way as above for toluene PLIF, the OH PLIF intensity is applied to represent the OH concentration. Color bars in Figs. 6 and 7 indicate the OH PLIF intensity level. The OH PLIF images in Figs. 6 and 7 have been subtracted with the background image recorded with the laser tuned off the resonance transition line.

The hollow core structure of the OH PLIF distribution indicated the location of the discharge channel. It is apparent that the OH molecules are localized in the vicinity of the discharge channel. The width of the OH region was measured to be around 8-11 mm, which is quite close to the effective width for toluene removal as measured from toluene PLIF images in Fig. 5. Comparing the intensity of OH PLIF signals shown in Figs. 6 and 7, it can be observed that the OH intensity increased in the presence of the toluene. Statistical analysis was performed to study the dependence of OH concentration on toluene concentration.

A square region (200 × 200 pixels, dashed square in Fig. 6) with the OH PLIF signals centralized, was selected for data analysis. The averaged OH PLIF intensity in this region is calculated by averaging over 200 single-shot frames and is used as an indicator of the OH concentrations. The dependence of this averaged OH PLIF intensity on the initial toluene concentration are shown in Fig. 8. Obviously, the OH concentration increases with the initial toluene concentration. The OH generation was enhanced by the increased toluene concentration. As higher concentrations of toluene was injected into the dicharge system, more OH radicals were formed through the reactions of toluene molecules with energetic electrons, ions and free radicals. Some possible reaction pathways for toluene decompositon were proposed as follow [19, 20, 31, 32].

$$C_6H_5{\cdot}CH_3 + e^- \rightarrow C_6H_5{\cdot}CH_2 + H + e^- \quad \text{(R11)}$$

$$O_2 + e^- \rightarrow O^- + O \quad \text{(R12)}$$

$$C_6H_5{\cdot}CH_3 + O^- \rightarrow C_6H_5{\cdot}CH_2 + OH + e^- \quad \text{(R13)}$$

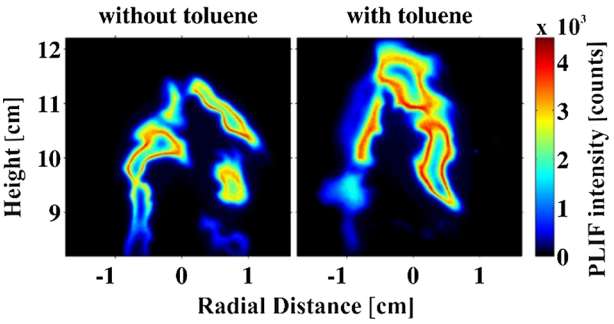

Fig. 7 Single-shot OH PLIF images recorded in the discharge for the flow without toluene and with 1.25% toluene contained, respectively. The laser sheet and the discharge system were aligned as in Configuration B

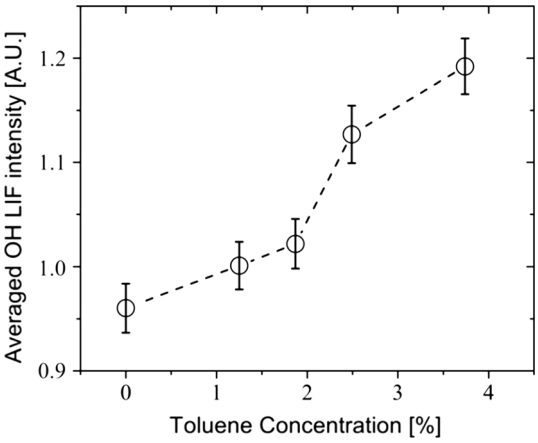

Fig. 8 Dependence of OH PLIF intensity on initial toluene concentration

$$O_2 + H \rightarrow OH + O \quad \text{(R14)}$$

$$C_6H_5{\cdot}CH_3 + OH + N_2 \rightarrow C_6H_5{\cdot}CH_3OH + N_2 \quad \text{(R15)}$$

$$C_6H_5{\cdot}CH_3 + OH \rightarrow C_6H_5{\cdot}CH_2 + H_2O \quad \text{(R16)}$$

According to R11 and R14, with the increase of toluene concentration, more H radicals will be abstracted from toluene molecules through reaction and OH will mainly be formed through oxygen derived radicals react with H. The trend that the OH generation increases with toluene concentration can be used to explain the findings in Fig. 4 that the absolute removal amount of toluene and energy efficiency increased with the increasing initial concentration under the fixed power.

Simultaneous OH and Toluene PLIF

To visualize the toluene decomposition process by the discharge channel directly, simultaneous OH and toluene PLIF measurements were carried out for an upward air stream with 1.25% toluene flowing across the gliding discharge channel, while the laser sheet was aligned as in configuration B. Figure 9 shows two pairs of simultaneous OH and toluene PLIF images from two typical cases. The 25% iso-intensity contours of OH PLIF have been plotted on top of the toluene PLIF images (red solid curves in Fig. 9b and d). Note that only the outer contours of the OH PLIF were plotted to visualize the outline of the active volume of the discharge channel.

It can be easily seen that, the distribution of the OH PLIF signal fitted quite well with the region where the toluene was removed in the toluene PLIF images. The good matching imply that OH played an important role in the toluene decomposition. To investigate the OH and toluene distribution in more detail, two parts with prominent structures have been selected for a cross sectional study as marked out with red dash circles in Fig. 9a. The cross-sectional intensity profiles are demonstrated along the white lines across the circle 1 and 2, respectively, with the results shown in Fig. 10. For each cross-sectional profile, the intensity values have been averaged for 10 pixels in vertical direction centered on the white dash lines.

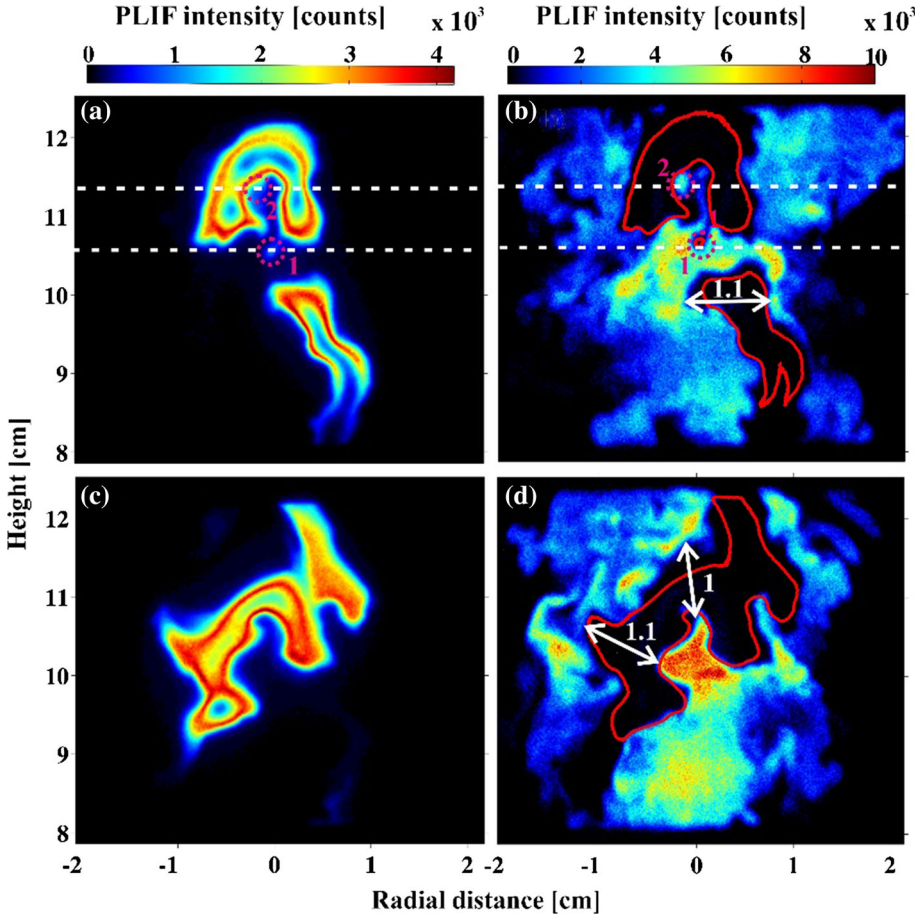

Fig. 9 Two pairs of simultaneous OH and toluene PLIF images from typical cases with toluene concentration of 1.25%. **a** and **c** OH PLIF images, **b** and **d** toluene PLIF images. The laser sheet and the discharge system were aligned as in Configuration B. *Red curve* shows the 25% iso-intensity contour of the OH PLIF. *White arrows* with numbers show the effective width in cm

As marked out by the red dash circle 1 in Fig. 9a, the OH PLIF intensity inside the circle 1 is only 25% of the maximum intensity, but it is still able to almost completely decompose the toluene (marked out with red circle in Fig. 9b). Figure 10a shows the cross sectional intenstity distribution across circle 1. It can be seen that the peak in the OH curve corresponding to the relatively low-intensity signal (25% of the maximum) inside circle 1 in Fig. 9a. Corresponding to this peak, the toluene PLIF signal was decreased down to 5% of the maximum. This fact demonstrate the powerful decomposing capability of the discharge channel. However, when the OH intensity is less than 20% of the maximum (marked out in circle 2), the capability of the discharge channel decomposing toluene drops substantially. Cross-sectional intensity distribution shown in Fig. 10b illustrates that the OH with 15% of maximum intensity cannot decompose the toluene adequately. Thus a toluene peak was left in the center which corresponds to the formed bulge (marked out by circle 2) in the toluene PLIF image Fig. 9b. It is also noticed that, the region where toluene removed have edges with high concentration gradient. This high toluene concentration

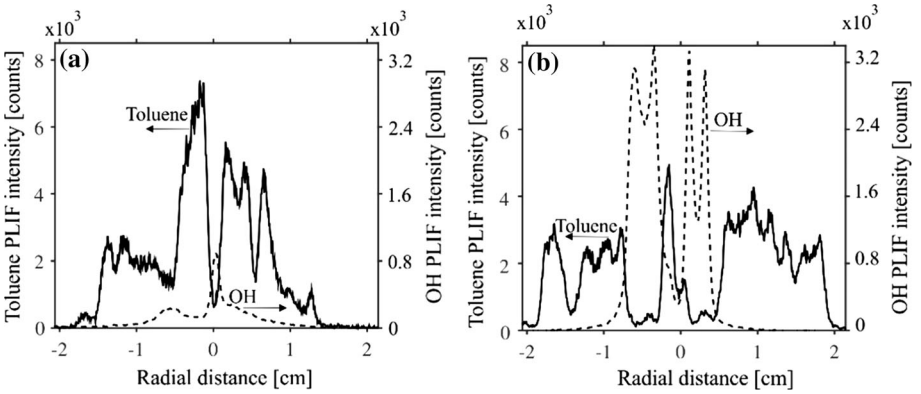

Fig. 10 Cross-sectional intensity profiles of simultaneous OH and toluene PLIF signals along the *white dash lines* across different circles in Fig. 9. **a** Circle 1; **b** Circle 2

gradient will enhance the diffusion of toluene molecules into the active volume of the discharge and lead to more decomposition.

The effective width of the active volume for toluene removal have been marked out with white arrows in Fig. 9. The effective width is estimated as the distance normal to the discharge channel, while the discharge channel is indicated by the hollow core of OH. Several examples of the effective width show that the width was around 1 cm. The good matching of OH and active volume indicate that the active volume of the discharge channel with capacity to decompose toluene was developed by the diffusion of reactive species like OH radicals. Previous studies [16, 17] have shown that OH could be effective in toluene destruction. A simulation of toluene destruction by an atmospheric pressure glow discharge conducted by Trushkin [20], even show that OH acts as a catalyst and the reaction of toluene with OH contribute the most in decomposition of $C_6H_5CH_3$ in the N_2:O_2:H_2O mixture. Thus it is suspected that the OH might play an important role in the toluene decomposition by gliding discharge as well. The main channels for OH initiate the decomposition of toluene are mainly through the reactions of R15 and R16 [20].Vigorous species like OH with high reactivity and relatively longer lifetime compared with electrons, can diffuse into a larger volume than the electrons to decompose the toluene molecules [33]. This is also the reason why the active volume for decomposing toluene has a larger radius than the luminous discharge channel. Note that, some parts of the toluene removed region have a larger width than the OH width. This suggest that there could be some other radicals responsible for the decomposition of the toluene. Some radicals with longer lifetimes or higher diffusivity, like O_3 and H, can diffuse into further than OH.

Even though the OH has a hollow structure, there exist high temperature and large number of energetic electrons and reactive ions in the center region of the arc channel [34]. Therefore, it is believed that the toluene would also be efficiently decomposed in the center region, so the effective width for toluene removal is reasonable to be estimated by the width of the OH distribution. Except for the decomposition of toluene, the other major source for OH radicals are from dissociation of water induced by electrons and atomic oxygen in humid air through R17 and R18 [35].

$$H_2O + e^- \rightarrow H + OH + e^- \quad \text{(R17)}$$

$$O + H_2O \rightarrow OH + OH \quad \text{(R18)}$$

Compared with direct initiating the toluene decomposition by O through R12, the interaction of OH and toluene molecules has a two orders of magnitude higher reaction rate. Thus the more important channel for O involved in the toluene destruction is a fast chain branching reaction R18 (time constant less than 10 ns), through which one O radical become two OH radicals. As discussed above, the active volume of the discharge channel is dominated by the production and diffusion of radicals from the discharge. To faciliatate the toluene removal efficiency by gliding discharge, it will be beneficial to generate more reactive radicals.

Conclusion

OH and toluene PLIF were performed simultaneously for on-line measurements of the removal process of toluene by a gliding arc discharge. Instantaneous visualization of the relative distribution of the removed toluene with the discharge channel were obtained. The planar toluene removal efficiency and instantaneous local removal efficiency of a single discharge channel were estimated from the averaged and single-shot toluene PLIF images, respectively. Under the fixed flow rate and supplied power of the gliding arc discharge system, it is found that the toluene removal efficiency was decreased with the inlet toluene concentration while the absolute amount of decomposing toluene increased.

OH PLIF studies showed that more OH radicals were produced when the initial toluene concentration increased. This suggests that the OH generation was enhanced by the decomposition of toluene molecules. This could be a hint for understanding the toluene decomposing mechanism and offering a promising path to promote toluene removal.

Simultaneous OH and toluene PLIF measurements showed that the OH PLIF region is complementary to the region where toluene was removed. The region of OH can be used as a marker of the active volume of the gliding discharge for toluene decomposition. The effective width of the active plasma volume is mainly determined by the diffusion of the reactive species. The effective width estimated from the toluene PLIF images is about 1 cm. To improve the overall removal efficiency of the discharge system, it would be preferable to promote the generation and diffusion of reactive species.

Overall, PLIF techniques provide a powerful tool to conduct in situ and non-intrusive investigations of the reaction system of pollutants and non-equilibrium discharges, gaining a better understanding of the toluene removal process. Development of the PLIF techniques to quantitative measurements of toluene and OH concentration and other active species should be further carried out, aiming at better understanding of the mechanism of the toluene treatment by the non-equilibrium discharges.

Acknowledgements The work was financially supported by the Swedish Energy Agency, the Knut & Alice Wallenberg foundation, the Swedish Research Council (VR) and the European Research Council (Advanced Grant TUCLA program). J. GAO would like to thank the financial support from the China Scholarship Council.

Compliance with Ethical Standards

Conflict of interest The authors declare that they have no conflict of interest.

References

1. Sobacchi M, Saveliev A, Fridman AA, Gutsol AF, Kennedy L (2003) Experimental assessment of pulsed corona discharge for treatment of VOC emissions. Plasma Chem Plasma Process 23(2):347–370. doi:10.1023/A:1022976204132
2. Xiao G, Xu WP, Wu RB, Ni MJ, Du CM, Gao X, Luo ZY, Cen KF (2014) Non-thermal plasmas for VOCs abatement. Plasma Chem Plasma Process 34(5):1033–1065. doi:10.1007/s11090-014-9562-0
3. Fridman A, Chirokov A, Gutsol A (2005) Non-thermal atmospheric pressure discharges. J Phys D Appl Phys 38(2):R1–R24. doi:10.1088/0022-3727/38/2/r01
4. vanVeldhuizen EM, Rutgers WR, Bityurin VA (1996) Energy efficiency of NO removal by pulsed corona discharges. Plasma Chem Plasma Process 16(2):227–247
5. Czernichowski A (1994) Gliding arc—applications to engineering and environment control. Pure Appl Chem 66(6):1301–1310. doi:10.1351/pac199466061301
6. Dalaine V, Cormier JM, Pellerin S, Lefaucheux P (1998) H2S destruction in 50 Hz and 25 kHz gliding arc reactors. J Appl Phys 84(3):1215–1221. doi:10.1063/1.368187
7. Du CM, Yan JH, Li XD, Cheron BG, You XF, Chi Y, Ni MJ, Cen KF (2006) Simultaneous removal of polycyclic aromatic hydrocarbons and soot particles from flue gas by gliding arc discharge treatment. Plasma Chem Plasma Process 26(5):517–525. doi:10.1007/s11090-006-9033-3
8. Cal MP, Schluep M (2001) Destruction of benzene with non-thermal plasma in dielectric barrier discharge reactors. Environ Prog 20(3):151–156. doi:10.1002/ep.670200310
9. Bo Z, Yan JH, Li XD, Chi Y, Cen KF (2008) Simultaneous removal of ethyl acetate, benzene and toluene with gliding arc gas discharge. J Zhejiang Univ Sci A 9(5):695–701. doi:10.1631/jzus.A071391
10. Zhu JJ, Sun ZW, Li ZS, Ehn A, Alden M, Salewski M, Leipold F, Kusano Y (2014) Dynamics, OH distributions and UV emission of a gliding arc at various flow-rates investigated by optical measurements. J Phys D Appl Phys. doi:10.1088/0022-3727/47/29/295203
11. Bo Z, Yan JH, Li XD, Chi Y, Cen KF (2008) Scale-up analysis and development of gliding arc discharge facility for volatile organic compounds decomposition. J Hazard Mater 155(3):494–501. doi:10.1016/j.jhazmat.2007.11.105
12. Burlica R, Kirkpatrick MJ, Locke BR (2006) Formation of reactive species in gliding arc discharges with liquid water. J Electrost 64(1):35–43. doi:10.1016/j.elstat.2004.12.007
13. Brisset JL, Moussa D, Doubla A, Hnatiuc E, Hnatiuc B, Youbi GK, Herry JM, Naitali M, Bellon-Fontaine MN (2008) Chemical reactivity of discharges and temporal post-discharges in plasma treatment of aqueous media: examples of gliding discharge treated solutions. Ind Eng Chem Res 47(16):5761–5781. doi:10.1021/ie701759y
14. Du CM, Yan JH, Cheron B (2007) Decomposition of toluene in a gliding arc discharge plasma reactor. Plasma Source Sci Technol 16(4):791–797. doi:10.1088/0963-0252/16/4/014
15. Leipold F, Fateev A, Kusano Y, Stenum B, Bindslev H (2006) Reduction of NO in the exhaust gas by reaction with N radicals. Fuel 85(10–11):1383–1388. doi:10.1016/j.fuel.2005.12.020
16. Bo Z, Yan JH, Li XD, Chi Y, Cen KF, Cheron BG (2007) Effects of oxygen and water vapor on volatile organic compounds decomposition using gliding arc gas discharge. Plasma Chem Plasma Process 27(5):546–558. doi:10.1007/s11090-007-9081-3
17. Lu SY, Sun XM, Li XD, Yan JH, Du CM (2012) Decomposition of toluene in a rotating glidarc discharge reactor. IEEE Trans Plasma Sci 40(9):2151–2156. doi:10.1109/tps.2012.2206119
18. Yu L, Li XD, Tu X, Wang Y, Lu SY, Yan JH (2010) Decomposition of Naphthalene by dc gliding arc gas discharge. J Phys Chem A 114(1):360–368. doi:10.1021/jp905082s
19. Trushkin AN, Kochetov IV (2012) Simulation of toluene decomposition in a pulse-periodic discharge operating in a mixture of molecular nitrogen and oxygen. Plasma Phys Rep 38(5):407–431. doi:10.1134/s1063780x12040083
20. Trushkin AN, Grushin ME, Kochetov IV, Trushkin NI, Akishev YS (2013) Decomposition of toluene in a steady-state atmospheric-pressure glow discharge. Plasma Phys Rep 39(2):167–182. doi:10.1134/s1063780x13020025
21. Koban W, Koch JD, Hanson RK, Schulz C (2005) Oxygen quenching of toluene fluorescence at elevated temperatures. Appl Phys B Lasers Opt 80(6):777–784. doi:10.1007/s00340-005-1769-6
22. Faust S, Goschutz M, Kaiser SA, Dreier T, Schulz C (2014) A comparison of selected organic tracers for quantitative scalar imaging in the gas phase via laser-induced fluorescence. Appl Phys B Lasers Opt 117(1):183–194. doi:10.1007/s00340-014-5818-x

23. Cheung BH, Hanson RK (2010) CW laser-induced fluorescence of toluene for time-resolved imaging of gaseous flows. Appl Phys B Lasers Opt 98(2–3):581–591. doi:10.1007/s00340-009-3785-4
24. Ehn A, Jonsson M, Johansson O, Aldén M, Bood J (2012) Quantitative oxygen concentration imaging in toluene atmospheres using dual imaging with modeling evaluation. Exp Fluids 54(1):1–8. doi:10.1007/s00348-012-1433-y
25. Sun ZW, Zhu JJ, Li ZS, Alden M, Leipold F, Salewski M, Kusano Y (2013) Optical diagnostics of a gliding arc. Opt Express 21(5):6028–6044
26. Zhu J, Gao J, Li Z, Ehn A, Aldén M, Larsson A, Kusano Y (2014) Sustained diffusive alternating current gliding arc discharge in atmospheric pressure air. Appl Phys Lett. doi:10.1063/1.4903781
27. Zhu J, Gao J, Ehn A, Li Z, Aldén M, Salewski M, Leipold F, Kusano Y (2014) Translational, rotational and vibrational temperatures of a gliding arc discharge at atmospheric pressure air. In: 14th international symposium on high pressure low temperature plasma chemistry
28. Kohno H, Berezin AA, Chang JS, Tamura M, Yamamoto T, Shibuya A, Honda S (1998) Destruction of volatile organic compounds used in a semiconductor industry by a capillary tube discharge reactor. Ind Appl IEEE Trans 34(5):953–966. doi:10.1109/28.720435
29. Pellerin S, Richard F, Chapelle J, Cormier JM, Musiol K (2000) Heat string model of bi-dimensional dc Glidarc. J Phys D Appl Phys 33(19):2407
30. Lee H, Chang M (2003) Abatement of gas-phase p-Xylene via dielectric barrier discharges. Plasma Chem Plasma Process 23(3):541–558. doi:10.1023/A:1023239122885
31. Ionin AA, Yu MK, Kozlov AY, Kotkov AA, Kochetov IV, Napartovich AP, Rulev OA, Seleznev LV, Sinitsyn DV, Vagin NP, Yuryshev NN (2009) Influence of nitrogen oxides NO and NO 2 on singlet delta oxygen production in pulsed discharge. J Phys D Appl Phys 42(1):015201
32. Vranckx S, Peeters J, Carl S (2008) A temperature dependence kinetic study of O(1D) + CH4: overall rate coefficient and product yields. Phys Chem Chem Phys 10(37):5714–5722. doi:10.1039/B804903C
33. Zheng CH, Shen X, Gao X, Li ZS, Zhu XB, Luo ZY, Cen KF (2013) planar laser-induced fluorescence diagnostics for spatiotemporal OH evolution in pulsed corona discharge. IEEE Trans Plasma Sci 41(3):485–493. doi:10.1109/tps.2013.2243919
34. Verreycken T, van der Horst RM, Baede AHFM, Van Veldhuizen EM, Bruggeman PJ (2012) Time and spatially resolved LIF of OH in a plasma filament in atmospheric pressure He–H_2O. J Phys D Appl Phys 45(4):045205
35. Benstaali B, Boubert P, Cheron B, Addou A, Brisset J (2002) Density and rotational temperature measurements of the OH and NO radicals produced by a gliding arc in humid air. Plasma Chem Plasma Process 22(4):553–571